Studying the Kondo Effect using Larsen's Pseudo-Fermions.

Bachelor Thesis

Written by *Stefan Sajin-Henningsen*

June 15, 2021

Supervised by
Jens Paaske

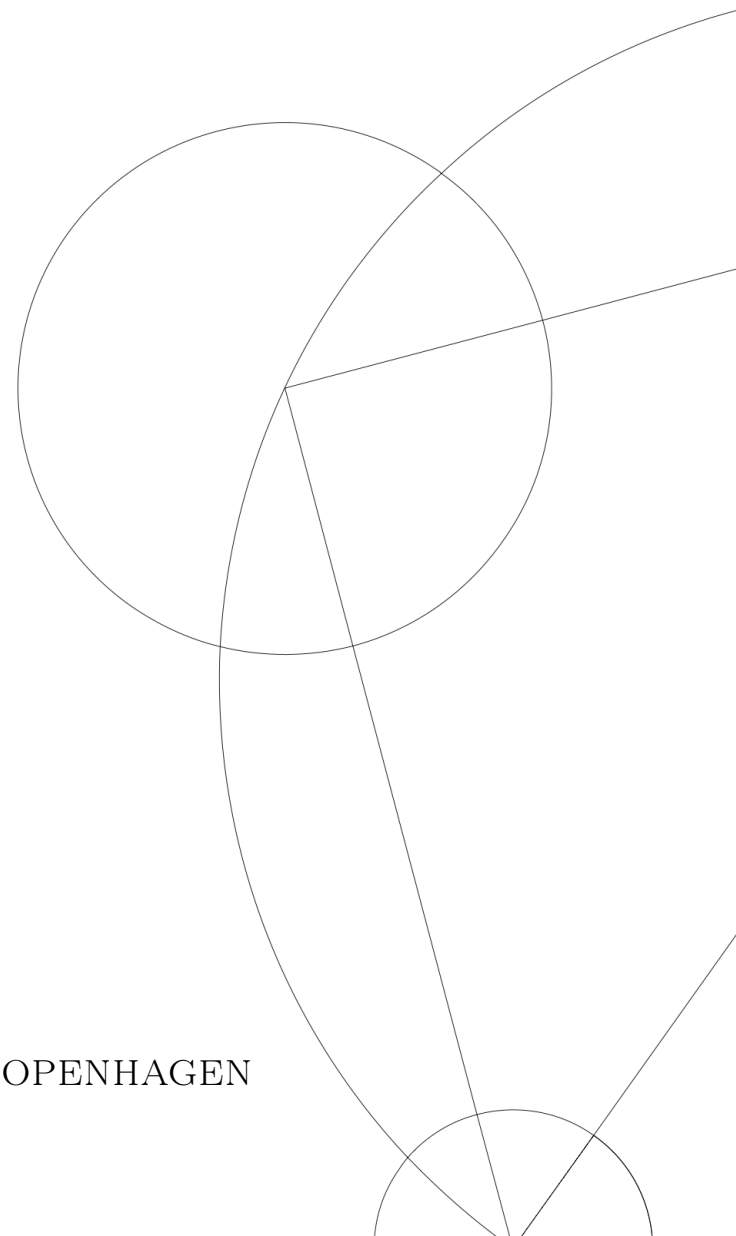

University of Copenhagen

UNIVERSITY OF
COPENHAGEN

Name of Institute:	Niels Bohr Institute
Name of Department:	Condensed Matter Theory
Author(s):	Stefan Sajin-Henningsen
Email:	rdw231@alumni.ku.dk
Title and subtitle:	Studying the Kondo Effect using Larsen's Pseudo-Fermions.
Supervisor(s):	Jens Paaske
Handed in:	15.06.2021
Defended:	22.06.2021

Name _____

Signature _____

Date _____

Contents

Abstract

A short introduction to the Kondo model and Keldysh formalism is given. Larsen's pseudo-fermions are introduced and used to derive the magnetization and transverse spin susceptibility of a toy-model. The toy-model consists of a single spin $\frac{1}{2}$ in a B-field. Both the derived magnetization and transverse spin susceptibility agree with well-known theory. Next, the impurity spin in the Kondo model is expressed in terms of Larsen's pseudo-fermions. Using this representation, the propagator of the conduction electrons is expanded perturbatively, and all contributions to the vertex up to 3. order in the coupling, g, are calculated. From this, 1-loop and 2-loop renormalization group (RG) results for the invariant coupling are derived. A divergence at a finite temperature T_K is seen to be present in 1-loop, but not in 2-loop RG. Finally, the strong coupling regime and the calculation of physical quantities are discussed, with special emphasis on why we should expect a divergence in the coupling g as $T \to 0$.

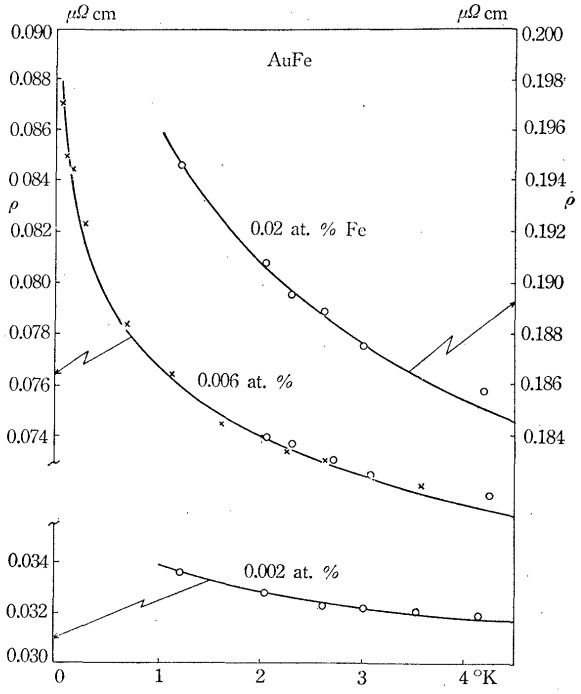

Figure 1: Resistivity ρ as a function of temperature T in AuFe for different concentrations of Fe. The figure is taken from Kondo's original article (1964) [1]. It is seen that the resistivity increases when lowering the temperature. The solid curve is a theoretical fit made by Kondo. It should be noted that in quantum dots it is not the resistivity, but the conductance, which increases as $T \to 0$.

1 Introduction

Many dilute alloys, consisting of a nonmagnetic metal that contains impurities with magnetic moments, show a minimum in their resistivity-temperature curve. This could be a dilute alloy such as AuFe. [1] Experiments show, that below a given temperature, the resistance of such an alloy increases when lowering the temperature further. This, somewhat surprising behavior, can be seen in fig. 1. In order to describe how this minimum of resistance can occur, Kondo introduced a model in 1964 [1], which later was named the Kondo model.

The Hamiltonian describing a metal with a Kondo impurity is given by

$$H = H_0 + H_K = \sum_{\mathbf{k}\sigma} \epsilon_{\mathbf{k}} c^\dagger_{\mathbf{k}\sigma} c_{\mathbf{k}\sigma} + \sum_{i,\mathbf{k}'\sigma'\mathbf{k}\sigma} J S^i c^\dagger_{\mathbf{k}'\sigma'} \tau^i_{\sigma'\sigma} c_{\mathbf{k}\sigma}, \tag{1.1}$$

where $\mathbf{S}$ is the spin of the impurity, $c^\dagger_{\mathbf{k}\sigma}$ creates an electron with momentum $\mathbf{k}$ and spin σ, τ is the vector of Pauli matrices and $\epsilon_{\mathbf{k}}$ is the energy of the conduction electrons, including the chemical potential μ. J is the interaction constant, which we will assume to be positive, i.e. antiferromagnetic. H_0 describes the energy of the conduction electrons (ce) and H_{K} is the exchange interaction which takes the spin of the impurity into account. It couples the conduction electrons indirectly, making this a many-body problem. Here we take the impurity concentration to be sufficiently small, such that we can neglect any impurity-impurity interaction.

The Kondo effect can not only be seen in bulk metals, but plays an important role in quantum dots and carbon nanotubes as well. [2] Even though much current research is concerned with these effects, we will focus on bulk metals here, since it is one of the simplest systems where one can observe the Kondo effect.

The following two sections give a short introduction to the formalism we will be using, with special emphasis on Larsen's pseudo-fermion (pf) representation. We will also use Larsen's pf's to study a spin $\frac{1}{2}$ in a B-field. It is a great warmup before moving to the more complex Kondo model.

2 Green's functions and Keldysh formalism

We will now derive a perturbative expansion for the ce-Green's function using Keldysh formalism. One of the strengths of Keldysh formalism is the simple form it takes in equilibrium as well as nonequilibrium problems. This is achieved by using contour integrals. Here we will only be working with the time-independent Hamiltonian H given in eq. 1.1, but the following can be generalized to include a time-dependent term in H as well.[1]

Let us start by writing the operators in the Heisenberg picture

$$\psi_H(1) = e^{iHt_1}\psi(0)e^{-iHt_1}, \tag{2.1}$$

where $1 \equiv (t_1, x_1)$. We can define averages as

$$\left\langle O_H(t)\right\rangle = \mathrm{Tr}[\rho(H)O_H(t)], \tag{2.2}$$

where O is the observable, H is the full Hamiltonian and $\rho = (\mathrm{Tr}\, e^{-\beta H})^{-1}e^{-\beta H}$ as usual. [3] For calculating physical quantities we will use Green's functions. For Fermi fields, ψ, we define the lesser and greater Green's function as

$$G^<(1,1') = +i\left\langle \psi_H^\dagger(1')\psi_H(1)\right\rangle \tag{2.3}$$

$$G^>(1,1') = -i\left\langle \psi_H(1)\psi_H^\dagger(1')\right\rangle, \tag{2.4}$$

respectively. [3]

We define contours and the contour-ordering operator T_c as follows: For a contour where t_1 is further along the contour than t_1', as seen on fig.2, we write $t_1 >_c t_1'$, such that

$$T_c(\psi_H(1)\psi_H^\dagger(1')) = \begin{cases} \psi_H(1)\psi_H^\dagger(1') & \text{if } t_1 >_c t_1' \\ -\psi_H^\dagger(1')\psi_H(1) & \text{if } t_1 <_c t_1' \end{cases}. \tag{2.5}$$

This allows us to connect contour-ordering to our previous Green's functions in the following way

$$G(1,1') \equiv -i\left\langle T_c(\psi_H(1)\psi_H^\dagger(1'))\right\rangle = \begin{cases} G^>(1,1') & \text{if } t_1 >_c t_1' \\ G^<(1,1') & \text{if } t_1 <_c t_1' \end{cases}. \tag{2.6}$$

We can now make a perturbative expansion of G upon noting that $e^{-\beta H} = e^{-\beta H_0}v(t_0 - i\beta, t_0)$, where

$$v(t,t_0) = T\exp\left[-i\int_{t_0}^{t} dt' H_{K,H_0}(t')\right]. \tag{2.7}$$

[1] This is beyond the scope of this thesis. See Rammer and Smith [3] for more on how this can be done.

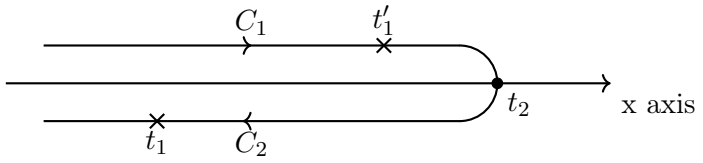

Figure 2: Keldysh contour for a propagator $G(1,1')$ where $t_1 >_c t_1'$. We will take $t_2 \to \infty$ so both the upper contour, C_1, and the lower contour, C_2, spans from $-\infty$ to ∞.

Here T is the time-ordering operator and H_{K,H_0} is H_K written in the interaction picture. [3] After some calculations[2] we get the following perturbative expansion of the full contour-ordered ce-Green's function of n'th order in J

$$\begin{aligned} G^{(n)}(\tau a, \tau' a') = -i\frac{(-i)^n}{n!2^n} J^n \int_c d\tau_1 \dots \int_c d\tau_n \sum_{i_1 \dots i_n} \sum_{\substack{\gamma_1 \dots \gamma_n \\ \gamma_1' \dots \gamma_n'}} \sum_{\substack{a_1 \dots a_n \\ a_1' \dots a_n'}} \tau^{i_1}_{\gamma_1' \gamma_1} \tau^{i_1}_{\sigma_1' \sigma_1} \dots \tau^{i_n}_{\gamma_n' \gamma_n} \tau^{i_n}_{\sigma_n' \sigma_n} \\ \times \left\langle T_c \left(f^\dagger_{\gamma_1'}(\tau_1) f_{\gamma_1}(\tau_1) \dots f^\dagger_{\gamma_n'}(\tau_n) f_{\gamma_n}(\tau_n) \right) \right\rangle_0 \\ \times \left\langle T_c \left(c^\dagger_{a_1'}(\tau_1) c_{a_1}(\tau_1) \dots c^\dagger_{a_n'}(\tau_n) c_{a_n}(\tau_n) c_a(\tau) c^\dagger_{a'}(\tau') \right) \right\rangle_0, \end{aligned} \tag{2.8}$$

where $a \equiv \mathbf{k}\sigma$ and $\langle\rangle_0$ is the average taken with respect to the non-interacting Hamiltonian H_0. Here we have written the impurity spin using Larsen's pf's. In the next section it will become clear how this is done. Now, upon applying Wick's theorem, we get

$$G^{(n)}(\tau a, \tau' a') = A^{(n)} \times \begin{vmatrix} [1,1'] & \dots & [1,n'] \\ \vdots & \ddots & \vdots \\ [n,1'] & \dots & [n,n'] \end{vmatrix} \times \begin{vmatrix} (a,a') & (a,1') & \dots & (a,n') \\ (1,a') & (1,1') & \dots & (1,n') \\ \vdots & \vdots & \ddots & \vdots \\ (n,a') & (n,1') & \dots & (n,n') \end{vmatrix}, \tag{2.9}$$

with $[a,a']$ and (a,a') being the free-particle contour ordered Green's functions for pf's and ce's respectively, and

$$A^{(n)} = (-1)^f \frac{i^n}{n!2^n} J^n \int_c d\tau_1 \dots \int_c d\tau_n \sum_{i_1 \dots i_n} \sum_{\substack{\gamma_1 \dots \gamma_n \\ \gamma_1' \dots \gamma_n'}} \sum_{\substack{a_1 \dots a_n \\ a_1' \dots a_n'}} \tau^{i_1}_{\gamma_1' \gamma_1} \tau^{i_1}_{\sigma_1' \sigma_1} \dots \tau^{i_n}_{\gamma_n' \gamma_n} \tau^{i_n}_{\sigma_n' \sigma_n}, \tag{2.10}$$

where f is the total number of ce- and pf-loops. Note that some factors of i have been absorbed into the free-particle Green's functions. The last step now is to go from contour integrals to time integrals. This can be done by noting that if we set $t_2 \to \infty$ in fig. 2, we can write

$$\int_c d\tau \to \int_{-\infty}^{\infty} dt - \int_{-\infty}^{\infty} dt, \tag{2.11}$$

and it is seen that we can go from contour ordering to time ordering by defining the propagators and vertices as tensors. From eq. 2.11 it is clear that the vertex must be given by

[2] We will not go into too much detail on how the perturbative expansion is done. But the main idea is to make a power expansion of v, and then the result follows readily.

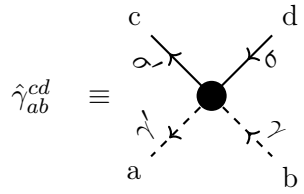

Figure 3: The Keldysh vertex is represented by a dot. Solid lines are ce-propagators and dashed lines are pf-propagators. Here a, b, c, d take the values 1 or 2 if they reside on the upper contour, C_1 or lower contour C_2 respectively. σ and γ describes the spin of the propagators as seen in eq. 2.8.

$$\hat{\gamma}^{cd}_{ab} = \frac{1}{2}\left(\delta_{ac}\tau^3_{bd} + \delta_{bd}\tau^3_{ac}\right) \xrightarrow{L\tau^3\gamma L^\dagger} \frac{1}{2}\left(\delta_{ab}\tau^1_{cd} + \delta_{cd}\tau^1_{ab}\right), \tag{2.12}$$

where τ^i is the i'th Pauli matrix, and all other symbols are clear from fig. 3. In the last step we have made the transformation $L\tau^3\gamma L^\dagger$, with $L = \frac{1}{\sqrt{2}}(\tau^0 - i\tau^2)$ and τ^0 being the 2×2 identity matrix. This is done because the propagators take a nice form under this transformation. [3] After some lengthy calculations, they are found to be given by

$$\begin{aligned}\underline{G} &= \begin{bmatrix} G^R(1,1') & G^K(1,1') \\ 0 & G^A(1,1') \end{bmatrix} \\ &= \begin{bmatrix} \theta(t_1 - t_1')(G^>(1,1') - G^<(1,1')) & G^>(1,1') + G^<(1,1') \\ 0 & -\theta(t_1' - t_1)(G^>(1,1') - G^<(1,1')) \end{bmatrix}. \end{aligned} \tag{2.13}$$

In this way we can go from contour integrals to time integrals, if we view the vertices and propagators as tensors. By going to the interaction picture, expanding the resulting Green's function and going to real time, we have now derived a perturbative expansion of the ce-Green's function. Next, let us take a closer look at Larsen's pseudo-fermions.

3 Larsen's pseudo-fermions

In order to study the Kondo model, we need to be able to describe the spin of the impurity. As Kondo showed, it is the dynamic nature of the spin, namely its commutation relations, which gives rise to the Kondo effect. [1] However, in order to use the formalism of Feynman diagrams and Wick's Theorem, we need to represent the impurity spin in terms of fermionic operators. This can be done in several ways. Here we will use one method given by Ulf Larsen. [4] It has the advantage that the pf's have zero chemical potential which simplifies the calculations. However, as we will see, spurious states can appear, and we have to deal with these.[3]

3.1 Formalism

We want to include the impurity spin in our Hamiltonian, while still being able to use standard methods of diagrammatic perturbation theory. This can be done by representing the impurity

[3] It should be noted that this representation only works for $S = \frac{1}{2}$ and $S = 1$, see [4] for more on this.

Pseudo-Fermion states for $S = \frac{1}{2}$			
n	State	S^z	$S \cdot S$
0	$\|\Omega\rangle$	0	0
1	$\|\uparrow\rangle$	$\frac{1}{2}$	$\frac{3}{4}$
1	$\|\downarrow\rangle$	$-\frac{1}{2}$	$\frac{3}{4}$
2	$\|\uparrow\downarrow\rangle$	0	0

Figure 4: All possible pf-states. Ω is the state with no pseudo-fermions present. The blue states are the spurious, unphysical, states. It is seen that all the unphysical states have $S \cdot S = 0$.

spin using pseudo-fermions. We will write the impurity spin as

$$S^i = \frac{1}{2} \sum_{\sigma' \sigma} f^\dagger_{\sigma'} \tau^i_{\sigma' \sigma} f_\sigma, \tag{3.1}$$

where $f^\dagger_\sigma$ and f_σ are creation and destruction operators of pseudo-fermions, which obey the usual fermion anticommutation rules

$$\left\{ f_\sigma, f^\dagger_{\sigma'} \right\} = \delta_{\sigma,\sigma'}, \qquad \{ f_\sigma, f_{\sigma'} \} = \left\{ f^\dagger_\sigma, f^\dagger_{\sigma'} \right\} = 0. \tag{3.2}$$

When using pseudo-fermions, we will generate unphysical states as seen in fig. 4. Hence we need a way to map statistical averages calculated in this extended Hilbert space to the physical averages, where we only take physical states into account. Let us write[4]

$$\langle \mathscr{R} \rangle^s = \langle \mathscr{R} \rangle^e \mathscr{A} \mathscr{L}, \tag{3.3}$$

with

$$\mathscr{A} = \frac{\mathrm{Tr}^s \left(e^{-\beta H} \mathscr{R} \right)}{\mathrm{Tr}^e \left(e^{-\beta H} \mathscr{R} \right)}, \qquad \mathscr{L} = \frac{\mathrm{Tr}^e \left(e^{-\beta H} \right)}{\mathrm{Tr}^s \left(e^{-\beta H} \right)} \equiv \frac{Z^e}{Z^s}, \tag{3.4}$$

where $\langle \mathscr{R} \rangle^e$ and $\langle \mathscr{R} \rangle^s$ are the average of the operator $\mathscr{R}$ calculated in the extended and physical Hilbert space, respectively. Note that

$$\mathrm{Tr}^e = \sum_{\{n\},\{A\}} \langle A | \langle n | ... | n \rangle | A \rangle = \sum_{\{A\}} \langle A | \sum_{n=0}^{2S+1} \mathrm{Tr}_n(...) | A \rangle \tag{3.5}$$

is the trace over all possible states, consisting of all subsets with n number of pseudo-fermions present. $\mathrm{Tr}_n(...)$ is the trace over all pf states containing exactly n pseudo-fermions, with $\sum_{\{A\}}$ tracing out any remaining degrees of freedom, such as the states of the conduction electrons. Tr^s is just the trace over physical states, i.e. states with $n = 1$.

If $\mathscr{R}$ can be written as a sum of products of $S_i ... S_j$ we get

$$\mathscr{A} = \frac{\mathrm{Tr}^s \left(e^{-\beta H} \mathscr{R} \right)}{\mathrm{Tr}^e \left(e^{-\beta H} \mathscr{R} \right)} = \frac{\mathrm{Tr}^s \left(e^{-\beta H} \mathscr{R} \right)}{\mathrm{Tr}^s \left(e^{-\beta H} \mathscr{R} \right)} = 1, \tag{3.6}$$

[4]The notation used here follows the one used by Larsen in his note [4] on pf's, where he also treats the $S = 1$ case.

since, for $S = \frac{1}{2}$, we have $\mathbf{S} \cdot \mathbf{S} = 0$ for the spurious pseudo-fermion states as seen from fig. 4. We will use this result in the next section, when we look at our toy model of a single spin 1/2 in a B-field.

Now, in order to use pf's with the Kondo model, let us see how one can go from extended to physical Hilbert space, when working with Green's functions for the conduction electrons. Here we look at the interaction H_K given in Eq. 1.1. Just like in eq. 2.6 we define

$$\begin{aligned} G(1,1') &= -i \left\langle T_c(\psi_H(1)\psi_H^\dagger(1')) \right\rangle \equiv \langle D \rangle \\ G_0(1,1') &= -i \left\langle T_c(\psi_{H_0}(1)\psi_{H_0}^\dagger(1')) \right\rangle_0 \equiv \langle D_0 \rangle_0 \,, \end{aligned} \tag{3.7}$$

where the average is taken in extended Hilbert space. Since D_0 does not depend on the pseudo-fermions,[5] we can write the physical Green's functions as

$$G^s = \langle D \rangle^s \,, \qquad G_0^s = \langle D_0 \rangle_0^s = \langle D_0 \rangle_0 = G_0, \tag{3.8}$$

where $\langle\rangle^s$ is the average taken w.r.t. all physical states, i.e. states containing exactly one pf. In order to map G to G^s we note that since the interaction term is zero for states with zero and two pf's, we can write the trace over all pf states as[6]

$$\begin{aligned} \mathrm{Tr}^e(\rho D) &= \sum_{\{A\}} \langle A| \,\mathrm{Tr}_0(\rho_0 D_0) + \mathrm{Tr}_1(\rho D) + \mathrm{Tr}_2(\rho_0 D_0)|A\rangle \\ &= \frac{1}{2}\,\mathrm{Tr}^e(\rho_0 D_0) + \mathrm{Tr}^s(\rho D). \end{aligned} \tag{3.9}$$

Defining $U = \rho_0^{-1}\rho$ such that $\langle U \rangle_0 = \frac{Z^e}{Z_0^e}$, we can write

$$\begin{aligned} \mathscr{A} &= \frac{\mathrm{Tr}^s(\rho D)}{\mathrm{Tr}^e(\rho D)} \\ &= 1 - \frac{\frac{1}{2}\,\mathrm{Tr}^e(\rho_0 D_0)}{\mathrm{Tr}^e(\rho D)} \\ &= 1 - \frac{G_0}{2G\,\langle U \rangle_0}. \end{aligned} \tag{3.10}$$

Now, from the definition of $\langle U \rangle_0$ and $\mathscr{L}$, it follows from 3.9 that

$$\mathscr{L} = \frac{2\,\langle U \rangle_0}{2\,\langle U \rangle_0 - 1}, \tag{3.11}$$

and we finally see from $G^s = G\mathscr{A}\mathscr{L}$ that

$$G^s - G_0^s = \mathscr{L}G - G_0 \left(\frac{\mathscr{L}}{2\,\langle U \rangle_0} + 1 \right) = \mathscr{L}(G - G_0). \tag{3.12}$$

[5] Here the coupling J is effectively zero, since we are using the non interacting Hamiltonian. See the comment following eq. 2.8.

[6] Note again that 0 in subscript on ρ simply means w.r.t. the non-interacting Hamiltonian. All notation should be clear from the above.

We can write this in terms of the $t-$matrix as

$$G^s - G_0^s = G_0^s t^s G_0^s, \qquad G - G_0 = G_0 t G_0. \tag{3.13}$$

This gives us

$$t^s = \mathscr{L} t, \tag{3.14}$$

which maps the $t-$matrix from extended to physical Hilbert space.[7]

3.2 Example on spin $\frac{1}{2}$ in a magnetic field

In order to get some feel for this new formalism, let us look at a toy model: A single spin $1/2$ in an external B-field. The B-field is constant in time and aligned parallel to the z-axis. We can write the Hamiltonian, H_{B}, in terms of pf's as

$$H_{\mathrm{B}} = \frac{B}{2} \sum_{\sigma'\sigma} f^\dagger_{\sigma'} \tau^3_{\sigma'\sigma} f_\sigma = \frac{B}{2} \left(f^\dagger_\uparrow f_\uparrow - f^\dagger_\downarrow f_\downarrow \right). \tag{3.15}$$

And again going to the Heisenberg picture, we can get the time dependence of the pf-operators

$$\frac{\partial f_\sigma(t)}{\partial t} = i[H_{\mathrm{B}}, f_\sigma](t) = -i \frac{\sigma B}{2} f_\sigma, \tag{3.16}$$

which yields

$$f_\sigma(t) = f_\sigma e^{-\frac{i\sigma B}{2} t}, \qquad f^\dagger_\sigma(t) = f^\dagger_\sigma e^{\frac{i\sigma B}{2} t}, \tag{3.17}$$

where $\sigma = \pm 1$ for spin up and down respectively. As noted earlier, we can map functions from the extended to the physical Hilbert space using the relation given in 3.3. For H_{B} given in eq. 3.15 we find

$$\mathscr{L} = \frac{\mathrm{Tr}^e \left(e^{-\beta H_0} \right)}{\mathrm{Tr}^s \left(e^{-\beta H_0} \right)} = \frac{2 + e^{\beta \frac{B}{2}} + e^{-\beta \frac{B}{2}}}{e^{\beta \frac{B}{2}} + e^{-\beta \frac{B}{2}}} = \frac{\left(1 + e^{\beta \frac{B}{2}}\right)\left(1 + e^{-\beta \frac{B}{2}}\right)}{e^{\beta \frac{B}{2}} + e^{-\beta \frac{B}{2}}}. \tag{3.18}$$

By noting that $\mathcal{G}_0(\sigma t, \sigma' t') = \mathcal{G}_0\left(\sigma, (t - t')\right) \delta_{\sigma\sigma'}$, we can get an expression for the greater Green's function

$$\begin{aligned} \mathcal{G}_0^{>}\left(\sigma, (t - t')\right) &= -i \left\langle f_\sigma(t) f^\dagger_\sigma(t') \right\rangle_0 \\ &= -i \left\langle f_\sigma f^\dagger_\sigma \right\rangle_0 e^{-i\frac{\sigma B}{2}(t - t')} \\ &= -i \left(1 - n_f \left(\frac{\sigma B}{2} \right) \right) e^{-i\frac{\sigma B}{2}(t - t')}, \end{aligned} \tag{3.19}$$

[7] The factor $\mathscr{L}$ can be quite difficult to calculate, and it might seem as a big drawback to using Larsen's pf's. Other methods, such as the pf's introduced by Abrikosov [5] eliminates unphysical states by including a chemical potential $\lambda \left(f^\dagger_\uparrow f_\uparrow + f^\dagger_\downarrow f_\downarrow \right)$ in the Hamiltonian. By taking λ to infinity, Abrikosov showed that the unphysical states got eliminated. He also showed that all diagrams containing more than one pf-loop, when calculating the ce-selfenergy, went to zero as $\lambda \to \infty$. However, taking this limit can introduce some even more serious complications. We will not go into more detail here, but it is important to note that when working with Larsen's pf's, we do not have to include an unphysical pf-potential in the Hamiltonian.

where $n_f(\epsilon) = \frac{1}{e^{\beta\epsilon}+1}$ is the Fermi function.

Since the Green's function given above only depends on the time difference $t-t'$, we will take the Fourier transform, and look at the retarded Green's function $\mathcal{G}^{\mathcal{R}}$. Here we add an infinitesimal part $i\eta$ to the frequency to ensure that the integral converges. After some calculations we get[8]

$$\mathcal{G}_0^R(\sigma,\omega) = \frac{1}{\omega - \epsilon_\sigma + i\eta}, \tag{3.20}$$

with $\epsilon_\sigma = \frac{\sigma B}{2}$. From this we can construct many new quantities, such as the spectral function

$$\mathcal{A}(\sigma,\omega) = 2\pi\delta(\omega - \epsilon_\sigma). \tag{3.21}$$

We can also get the lesser and greater Green's function by using the relation

$$\mathcal{G}_0^<(\sigma,\omega) = i\mathcal{A}(\sigma,\omega) n_f(\omega), \tag{3.22}$$
$$\mathcal{G}_0^>(\sigma,\omega) = -i\mathcal{A}(\sigma,\omega)\left(1 - n_f(\omega)\right). \tag{3.23}$$

We will see these quantities again, when working with the Kondo model.

We can now map physical quantities such as the magnetization M_0 to real Hilbert space by using eq. 3.3, 3.6 and 3.18

$$\begin{aligned} M_0 = \langle S^z\rangle_0^s = \mathscr{L}\langle S^z\rangle_0^{(e)} &= \frac{1}{2}\mathscr{L}\left(\left\langle f_\uparrow^\dagger f_\uparrow\right\rangle_0^{(e)} - \left\langle f_\downarrow^\dagger f_\downarrow\right\rangle_0^{(e)}\right) \\ &= \frac{-i}{2}\mathscr{L}\left(\mathcal{G}_0^<(\uparrow, t=0) - \mathcal{G}_0^<(\downarrow, t=0)\right) \\ &= \frac{1}{2}\frac{\left(1+e^{\beta\frac{B}{2}}\right)\left(1+e^{-\beta\frac{B}{2}}\right)}{e^{\beta\frac{B}{2}} + e^{-\beta\frac{B}{2}}}\left(n_f(\epsilon_\uparrow) - n_f(\epsilon_\downarrow)\right) \\ &= -\frac{1}{2}\tanh\left(\frac{\beta B}{2}\right), \end{aligned} \tag{3.24}$$

which is a well-known result for a spin $\frac{1}{2}$ in an external magnetic field. It is seen that multiplying by $\mathscr{L}$ effectively makes $\tanh\left(\frac{x}{2}\right) \to \tanh(x)$.
To get an even better understanding for this framework, let us look at the magnetic susceptibility of the spin $\frac{1}{2}$ next.

3.2.1 Calculating the transverse spin susceptibility for the toy model

We will now calculate the magnetic susceptibility, χ^{ij}, where $i,j \in \{x,y,z\}$. Inspired by eq. 2.6 we define it as [6]

$$\begin{aligned} \chi_0^{ij}(\tau,\tau') &= -i\left\langle T_c\left(S^i(\tau)S^j(\tau')\right)\right\rangle_0 \\ &= -i\left\langle T_c\left(\frac{1}{2}\sum_{\sigma'\sigma} f_{\sigma'}^\dagger(\tau)\tau^i_{\sigma'\sigma} f_\sigma(\tau)\frac{1}{2}\sum_{\eta'\eta} f_{\eta'}^\dagger(\tau')\tau^i_{\eta'\eta} f_\eta(\tau')\right)\right\rangle_0, \end{aligned} \tag{3.25}$$

[8]Here we look at the retarded Green's function similar to the one defined in eq. 2.13.

where we have used the definition of Larsen's pf's from eq. 3.1. Upon evaluating this using Wick's theorem, just as we did in eq. 2.9, we get

$$\begin{aligned}\chi_0^{ij}(\tau,\tau') &= -i\left\langle T_c\left(S^i(\tau)S^j(\tau')\right)\right\rangle_0 \\ &= -\frac{i}{4}\sum_{\sigma,\sigma'}\left[\tau^i_{\sigma',\sigma}\mathcal{G}_0(\sigma,\tau,\tau')\tau^j_{\sigma,\sigma'}\mathcal{G}_0(\sigma',\tau',\tau)\right] + \frac{i}{4}\sum_{\sigma}\left[\tau^i_{\sigma,\sigma}\mathcal{G}_0(\sigma,\tau,\tau)\right]\sum_{\sigma'}\left[\tau^j_{\sigma',\sigma'}\mathcal{G}_0(\sigma',\tau',\tau')\right].\end{aligned} \tag{3.26}$$

Here we have used the fact that the propagators are proportional to $\delta_{\sigma\sigma'}$ so they can be written as $G_0(\sigma,\tau',\tau)$.

As an example, let us calculate the retarded transverse spin susceptibility. We will see that it contains some new physics, compared to the magnetization we calculated earlier. The retarded transverse spin susceptibility is defined as

$$\begin{aligned}\chi_0^{\perp}(\tau,\tau') &= -i\left\langle T_c\left(S_-(\tau)S_+(\tau')\right)\right\rangle \\ &= \left(\chi_0^{xx}(\tau,\tau')+\chi_0^{yy}(\tau,\tau')+i\chi_0^{xy}(\tau,\tau')-i\chi_0^{yx}(\tau,\tau')\right),\end{aligned} \tag{3.27}$$

where $S_\pm = S_x \pm iS_y$ as usual. We now have to calculate the relevant χ^{ij}. It is seen from eq. 3.26 that

$$\chi_0^{xx}(\tau,\tau') = \chi_0^{yy}(\tau,\tau') = -\frac{i}{4}\left(\mathcal{G}_0(\uparrow,\tau,\tau')\mathcal{G}_0(\downarrow,\tau',\tau)+\mathcal{G}_0(\downarrow,\tau,\tau')\mathcal{G}_0(\uparrow,\tau',\tau)\right) \tag{3.28}$$

$$\chi_0^{xy}(\tau,\tau') = -\chi_0^{yx}(\tau,\tau') = -\frac{1}{4}\left(\mathcal{G}_0(\uparrow,\tau,\tau')\mathcal{G}_0(\downarrow,\tau',\tau)-\mathcal{G}_0(\downarrow,\tau,\tau')\mathcal{G}_0(\uparrow,\tau',\tau)\right). \tag{3.29}$$

An easy way to go from contour to real times is to use Langreth Theorem. [7] This theorem states that given an expression of the from $C(\tau,\tau') = A(\tau,\tau')B(\tau',\tau)$, the retarded component is given by

$$C^R(t,t') = A^R(t,t')B^<(t',t) + A^<(t,t')B^A(t',t). \tag{3.30}$$

Noting $\mathcal{G}_0(\sigma,\tau,\tau') = \mathcal{G}_0(\sigma,\tau-\tau')$ we can perform the Fourier Transform w.r.t $t-t'$, and using the expression for $\mathcal{G}$ given in eq. 3.22, we get the convolution

$$\begin{aligned}\chi_0^{xx,R}(\omega) &= -\frac{i}{4}\int\frac{d\omega'}{2\pi}\Big(\mathcal{G}_0^R(\uparrow,\omega')\mathcal{G}_0^<(\downarrow,\omega'-\omega)+\mathcal{G}_0^<(\uparrow,\omega')\mathcal{G}_0^A(\downarrow,\omega'-\omega) \\ &\qquad +\mathcal{G}_0^R(\downarrow,\omega')\mathcal{G}_0^<(\uparrow,\omega'-\omega)+\mathcal{G}_0^<(\downarrow,\omega')\mathcal{G}_0^A(\uparrow,\omega'-\omega)\Big) \\ &= -\frac{i}{4}\int\frac{d\omega'}{2\pi}\left(\frac{2i\pi\delta(\omega'-\omega+\frac{B}{2})n_f\left(\omega'-\omega\right)}{\omega'-\frac{B}{2}+i\eta}+\frac{2i\pi\delta(\omega'-\frac{B}{2})n_f\left(\omega'\right)}{\omega'-\omega+\frac{B}{2}-i\eta}\right. \\ &\qquad \left.+\frac{2i\pi\delta(\omega'-\omega-\frac{B}{2})n_f\left(\omega'-\omega\right)}{\omega'+\frac{B}{2}+i\eta}+\frac{2i\pi\delta(\omega'+\frac{B}{2})n_f\left(\omega'\right)}{\omega'-\omega-\frac{B}{2}-i\eta}\right) \\ &= \frac{n_f(\frac{B}{2})-n_f(\frac{-B}{2})}{4}\left(\frac{1}{\omega+B+i\eta}-\frac{1}{\omega-B+i\eta}\right).\end{aligned} \tag{3.31}$$

Now, going through the same steps for χ_0^{xy}, we get

$$\chi_0^{xy,R}(\omega) = i\frac{n_f(\frac{B}{2})-n_f(\frac{-B}{2})}{4}\left(\frac{1}{\omega+B+i\eta}+\frac{1}{\omega-B+i\eta}\right). \tag{3.32}$$

Using these results in eq. 3.27 we end up with

$$\begin{aligned}\chi_0^{\perp,R}(\omega) &= \left(2\chi_0^{xx}(\tau,\tau') + 2i\chi_0^{xy}(\tau,\tau')\right) \\ &= \frac{n_f(\frac{B}{2}) - n_f(\frac{-B}{2})}{2}\left(\frac{1}{\omega+B+i\eta} - \frac{1}{\omega-B+i\eta} - \frac{1}{\omega+B+i\eta} - \frac{1}{\omega-B+i\eta}\right) \\ &= -\frac{n_f(\frac{B}{2}) - n_f(\frac{-B}{2})}{\omega-B+i\eta}. \end{aligned} \tag{3.33}$$

And mapping to physical Hilbert space using eq. 3.18 we get the result

$$\begin{aligned}\chi_0^{\perp,R}(\omega) &= -\mathscr{L}\frac{n_f(\frac{B}{2}) - n_f(\frac{-B}{2})}{\omega-B+i\eta} \\ &= -\frac{\left(1+e^{\beta\frac{B}{2}}\right)\left(1+e^{-\beta\frac{B}{2}}\right)}{e^{\beta\frac{B}{2}}+e^{-\beta\frac{B}{2}}}\frac{n_f(\frac{B}{2}) - n_f(\frac{-B}{2})}{\omega-B+i\eta} \\ &= \tanh\left(\frac{\beta B}{2}\right)\left(\frac{1}{\omega-B+i\eta}\right), \end{aligned} \tag{3.34}$$

which is the result we expect for a spin $\frac{1}{2}$ in an external magnetic field.

We could include a finite lifetime of the spin. This can be useful when going to the strong coupling regime of the Kondo model. The pf-propagator is then given as in eq. 5.1, and we would expect the divergence at $\omega = B$ to get broadened by the parameter Γ. The calculations go like the ones above, but using the new expression for G instead. But the resulting integrals are now more complicated, and we will not try to perform them here.

However, to get a deeper understanding for the physics that the transverse susceptibility describes, let us write it in real time as

$$\chi_0^{\perp,R}(t) = -i\theta(t)\left\langle[S_-(t), S_+(0)]\right\rangle, \tag{3.35}$$

from which we see that the transverse susceptibility contains information about the dynamics of the spin. If the spin did not have any internal degrees of freedom, and no dynamics, this commutator would be zero. However, when the energy of the two spin states are far from each other compared to the temperature, and we look at frequencies close to the energy difference between these two states, the transverse susceptibility $\chi_0^{\perp,R}(\omega)$ can become large, and even diverge.[9] Actually, it is exactly the fact that $[S_-(t), S_+(0)] \neq 0$ in general, that gives rise to the Kondo effect as we will see later. This is also described by Kondo in his article from 1964 [1]. With our newfound understanding of Keldysh formalism and Larsen's pf's, we are now ready to deal with the Kondo model.

4 The Kondo model in the weak coupling regime

We will study the Kondo model in the weak coupling regime, that is, for temperatures T greater than T_K.[10] Our goal is to calculate the effective, dimensionless coupling constant $g = J\nu$, where

[9] It is clear that by including Γ in our pf-propagator, we can get rid of the divergence at $\omega = B$. We will see how this finite lifetime can arise in bulk metals later.

[10] T_K is the Kondo temperature to be defined later.

ν is the ce-density of states at the Fermi surface. The coupling plays an important role when calculating physical quantities such as the resistivity of the metal. But it also gives a great insight to how the diagrammatic works out when using Larsen's pf's. Finally, the vertex shows some fascinating behavior itself. Depending on which type of diagrams we sum up, different divergences occur. When summing up infinite series of diagrams, methods from the Renormalization Group will prove to be very useful, as we will see shortly.

4.1 Vertex diagrams

In fig. 5 all contributions to the vertex up to third order in g are shown.

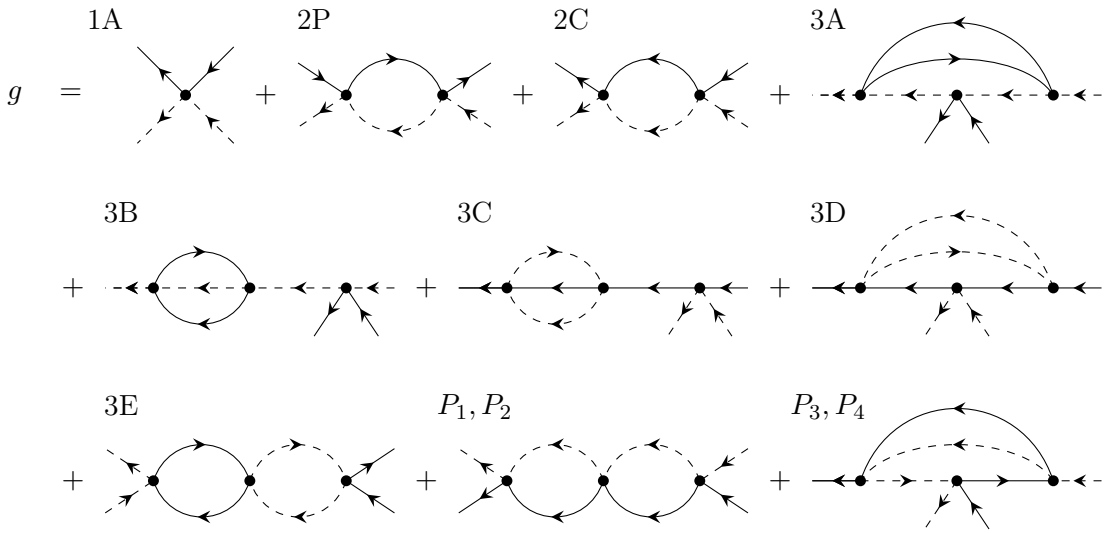

Figure 5: All 1., 2. and 3. order contributions to the vertex g are shown. $2P$ and $2C$ are parquet diagrams. P_1 is made by combining two $2C$-type diagrams. We have not shown P_2 which is made by combining two $2P$-type diagrams. P_3 and P_4 are made by combining one $2P$- and one $2C$-diagram. Again only one of the two possible diagrams is shown. As noted earlier solid and dashed lines correspond to ce- and pf-propagators, respectively.

Now that we have drawn all the diagrams, we have to do some calculations. We will use the perturbative expansion given in eq. 2.9, the Keldysh-vertex given in eq. 2.12 and the ce- and pf-propagators given by [11]

$$\underline{G}(\omega, p) = \begin{bmatrix} \frac{1}{\omega - \epsilon_p + i\eta} & (-2\pi i)\mathrm{sgn}(\epsilon_p) N_0 \delta(\omega - \epsilon_p) \\ 0 & \frac{1}{\omega - \epsilon_p - i\eta} \end{bmatrix} \tag{4.1}$$

$$\underline{\tilde{G}}(\omega) = \begin{bmatrix} \frac{1}{\omega + i\eta} & 0 \\ 0 & \frac{1}{\omega - i\eta} \end{bmatrix}. \tag{4.2}$$

Note that setting the pf-chemical potential to zero makes $\tilde{G}^K = 0$. As we will see, this puts some restrictions on which diagrams we need to include, when calculating the vertex corrections.

[11] This can be derived using eq. 2.13 and going thorugh the same steps as we did when deriving eq. 3.20. It shoud be noted that we assume $T \to 0$ here, so that we can write $n_f(-\epsilon_p) - n_f(\epsilon_p) = \mathrm{sgn}(\epsilon_p)$. This is only used in the Keldysh component, since it is this component which contains information about the occupation of the given state.

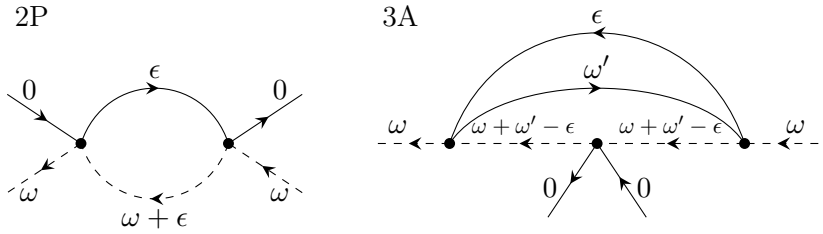

Figure 6: Example on how to attach frequencies to the propagators. Note that the incoming pf-propagator has an external frequency. We could have given the ce-propagator one as well, but this is not necessary as noted in the text.

4.2 2. order diagrams

Let us start by looking at the two parquet diagrams. These are the 2. order diagrams. We will only look at g^{21}_{11}, but g^{11}_{21} can be calculated in very much the same way. We will calculate the first diagram, 2P, in detail. Including a factor of $\frac{i}{4}\sum_k \tau^k_{\sigma'\sigma}\tau^k_{\gamma'\gamma}$ on the left hand side,[12] and introducing an UV-cutoff Λ on the ce-band,[13] we see from fig. 6 that[14]

$$
\begin{aligned}
&g^{(2P)}{}^{21}_{11}(\omega)\frac{i}{4}\sum_k \tau^k_{\sigma'\sigma}\tau^k_{\gamma'\gamma} \\
&\quad= \left(\frac{i}{4}\right)^2 \sum_{i_1,i_2}\left[\tau^{i_2}\tau^{i_1}\right]_{\gamma'\gamma}\left[\tau^{i_1}\tau^{i_2}\right]_{\sigma'\sigma}\int d\epsilon_p \int \frac{d\epsilon}{2\pi} g^2 (2\hat{\gamma}^{c'1}_{1b'})\underline{G}^{d'c'}(\epsilon,\epsilon_p)\underline{\tilde{G}}^{b'a'}(\omega+\epsilon)(2\hat{\gamma}^{2d'}_{a'1}) \\
&\quad= \frac{(-1)}{16}\sum_k \left(\delta_{\gamma'\gamma}\delta_{\sigma'\sigma} + 2\tau^k_{\sigma'\sigma}\tau^k_{\gamma'\gamma}\right)\int d\epsilon_p \int \frac{d\epsilon}{2\pi} g^2 \tilde{G}^R(\omega+\epsilon)G^K(\epsilon,\epsilon_p) \\
&\quad= \frac{(-1)}{16}\sum_k \left(\delta_{\gamma'\gamma}\delta_{\sigma'\sigma} + 2\tau^k_{\sigma'\sigma}\tau^k_{\gamma'\gamma}\right) \\
&\qquad \int d\epsilon_p \int \frac{d\epsilon}{2\pi} g^2 \frac{1}{\omega+\epsilon+i\eta}(-2\pi i)\mathrm{sgn}(\epsilon_p)\theta(\Lambda-|\epsilon_p|)\delta(\epsilon-\epsilon_p) \\
&\quad= \frac{i}{16}\sum_k \left(\delta_{\gamma'\gamma}\delta_{\sigma'\sigma} + 2\tau^k_{\sigma'\sigma}\tau^k_{\gamma'\gamma}\right)\int_{-\Lambda}^{\Lambda} d\epsilon_p g^2 \frac{1}{\omega+\epsilon_p+i\eta}\mathrm{sgn}(\epsilon_p) \\
&\quad= \frac{i}{16}\sum_k \left(\delta_{\gamma'\gamma}\delta_{\sigma'\sigma} + 2\tau^k_{\sigma'\sigma}\tau^k_{\gamma'\gamma}\right) g^2 \ln\left|\frac{\omega^2-\Lambda^2}{\omega^2}\right|. \qquad (4.3)
\end{aligned}
$$

The contribution from $g^{(2C)}$ can be found in the same way, and we get

$$
g^{(2C)}{}^{21}_{11}(\omega)\frac{i}{4}\sum_k \tau^k_{\sigma'\sigma}\tau^k_{\gamma'\gamma} = \frac{i}{16}\sum_k \left(-\delta_{\gamma'\gamma}\delta_{\sigma'\sigma} + 2\tau^k_{\sigma'\sigma}\tau^k_{\gamma'\gamma}\right) g^2 \ln\left|\frac{\omega^2-\Lambda^2}{\omega^2}\right|. \qquad (4.4)
$$

[12] We get i from the perturbative expansion, $\frac{1}{2}$ from the impurity spin, $\frac{1}{2}$ from the Keldysh vertex and a spin sum from H_K.

[13] The cutoff Λ is essential when doing our RG-calculations.

[14] Here we have suppressed the frequency-dependence of the vertices on the right hand side. It should be noted that we could have included a frequency in the incoming and outgoing ce-propagator as well. However, this would not change the final result in any way, since we take the limit of all external frequencies going to zero in the end, when doing the RG-calculations later.

It is seen that the terms containing $\delta_{\gamma'\gamma}\delta_{\sigma'\sigma}$ cancel out, and we end up with

$$g^{(2)}{}^{21}_{11}(\omega) = 2g^2 \ln\left|\frac{\Lambda}{\omega}\right|. \tag{4.5}$$

We will later use ideas from the Renormalization Group to make our vertex independent of the UV-cutoff Λ.

4.3 3. order diagrams

4.3.1 Diagram 3A and 3B

We can do exactly the same type of calculations for the third order diagrams. For diagram $3A$, using fig. 6, we get[15]

$$\begin{aligned}
&g^{(3A)}{}^{21}_{11}(\omega)\frac{i}{4}\sum_k \tau^k_{\sigma'\sigma}\tau^k_{\gamma'\gamma} \\
&\quad= \left(\frac{i}{4}\right)^3 (-1)\sum_{i_1,i_2,i_3}\left[\tau^{i_1}\tau^{i_2}\tau^{i_3}\right]_{\gamma'\gamma}\mathrm{Tr}\left[\tau^{i_1}\tau^{i_3}\right]\tau^{i_2}_{\sigma'\sigma}\int d\epsilon_p\int d\epsilon_q\int\frac{d\epsilon}{2\pi}\int\frac{d\omega'}{2\pi}g^3 \\
&\quad\Big[\Big(\tilde{G}^R(\omega+\omega'-\epsilon)\tilde{G}^R(\omega+\omega'-\epsilon)\Big)\Big(G^R(\omega',\epsilon_p)G^A(\epsilon,\epsilon_q) \\
&\qquad +G^A(\omega',\epsilon_p)G^R(\epsilon,\epsilon_q)+G^K(\omega',\epsilon_p)G^K(\epsilon,\epsilon_q)\Big) \\
&\quad+\Big(\tilde{G}^A(\omega+\omega'-\epsilon)\tilde{G}^A(\omega+\omega'-\epsilon)\Big)\Big(G^R(\omega',\epsilon_p)G^R(\epsilon,\epsilon_q)+G^A(\omega',\epsilon_p)G^A(\epsilon,\epsilon_q)\Big)\Big].
\end{aligned} \tag{4.6}$$

After some lengthy calculations, which can be seen in appendix 8.1, we end up with

$$g^{(3A)}{}^{21}_{11}(\omega)\frac{i}{4}\sum_k \tau^k_{\sigma'\sigma}\tau^k_{\gamma'\gamma} = \left(\frac{i}{4}\right)^3\sum_k\left(2\tau^k_{\sigma'\sigma}\tau^k_{\gamma'\gamma}\right)g^3\left(2\ln\left|\frac{\Lambda^2-\omega^2}{\omega^2}\right|-2\ln\left|\frac{4\Lambda^2-\omega^2}{\Lambda^2-\omega^2}\right|\right). \tag{4.7}$$

Going through the same kind of calculations for diagram 3B, we get

$$g^{(3B)}{}^{21}_{11}(\omega)\frac{i}{4}\sum_k \tau^k_{\sigma'\sigma}\tau^k_{\gamma'\gamma} = \left(\frac{i}{4}\right)^3(-1)\sum_k\left(6\tau^k_{\sigma'\sigma}\tau^k_{\gamma'\gamma}\right)g^3\left(4\ln|2|-4\ln\left|\frac{\Lambda}{\omega}\right|\right). \tag{4.8}$$

None of the other diagrams come with logarithmic contributions as we will see shortly. So to third order in g, keeping track of log-diagrams only, we get the following correction to the vertex

$$\begin{aligned}
g^{(3)}{}^{21}_{11}(\omega) &= \left(\frac{i}{4}\right)^2 g^3\left(4\ln\left|\frac{\Lambda^2-\omega^2}{\omega^2}\right|-4\ln\left|\frac{4\Lambda^2-\omega^2}{\Lambda^2-\omega^2}\right|-24\ln|2|+24\ln\left|\frac{\Lambda}{\omega}\right|\right) \\
&\to (-1)\frac{g^3}{16}\left(8\ln\left|\frac{\Lambda}{\omega}\right|-8\ln|2|-24\ln|2|+24\ln\left|\frac{\Lambda}{\omega}\right|\right) \\
&= g^3\left(2\ln|2|-2\ln\left|\frac{\Lambda}{\omega}\right|\right),
\end{aligned} \tag{4.9}$$

where we have taken the limit $\frac{\omega}{\Lambda}\to 0$ since Λ is an UV-cutoff.

[15] The (-1) comes form the ce-loop.

4.3.2 Diagram 3C, 3D, 3E

We will now look at the diagrams containing one pf-loop. If we had used Abrikosov's pf's we would expect these to be zero,[16] but this is not true when using Larsen's pf's.

When the ce- or pf-propagators make a closed loop, we get a trace over the propagators due to the Keldysh structure. Since $\underline{\tilde{G}}$ is diagonal, in order for the trace over the pf-loop to be non-zero, we need an equal number of τ^1's from the Keldysh vertices to get contracted with the pf-propagators in the loop. This restricts the non-zero terms that can be generated, when performing the contraction over Keldysh vertices. For diagram 3C in fig. 5 we get

$$\begin{aligned} g^{(3C)}{}^{21}_{11}(\omega) = \left(\frac{i}{4}\right)^3 (-1) \sum_k \left(6\tau^k_{\sigma'\sigma}\tau^k_{\gamma'\gamma}\right) \int d\epsilon_p \int d\epsilon_q \int \frac{d\epsilon}{2\pi} \int \frac{d\omega'}{2\pi} g^3 \\ \Big[\Big(\tilde{G}^R(\epsilon)\tilde{G}^R(\omega') + \tilde{G}^A(\epsilon)\tilde{G}^A(\omega')\Big) \\ \Big(G^K(\omega+\omega'-\epsilon,\epsilon_p)G^K(\omega,\epsilon_q) + G^R(\omega+\omega'-\epsilon,\epsilon_p)G^A(\omega,\epsilon_q)\Big) \\ + \Big(\tilde{G}^R(\epsilon)\tilde{G}^A(\omega') + \tilde{G}^A(\epsilon)\tilde{G}^R(\omega')\Big) G^A(\omega+\omega'-\epsilon,\epsilon_p)G^A(\omega,\epsilon_q)\Big]. \end{aligned} \tag{4.10}$$

The first part of the first term is zero for $\omega \to 0$ since $G^K(0,\epsilon_q) = 0$, and setting all terms with poles in only the lower or upper half-plane to zero, we end up with

$$\begin{aligned} g^{(3C)}{}^{21}_{11}(\omega) &= \left(\frac{i}{4}\right)^3 (-1) \sum_k \left(6\tau^k_{\sigma'\sigma}\tau^k_{\gamma'\gamma}\right) \\ &\int d\epsilon_p \int d\epsilon_q \int \frac{d\epsilon}{2\pi} \int \frac{d\omega'}{2\pi} g^3 \tilde{G}^A(\epsilon)\tilde{G}^R(\omega')G^A(\omega+\omega'-\epsilon,\epsilon_p)G^A(\omega,\epsilon_q) \\ &\propto \int d\epsilon_p \int d\epsilon_q \int d\epsilon \int d\omega' \left(\frac{1}{\epsilon - i\eta}\right)\left(\frac{1}{\omega' + i\eta}\right)\left(\frac{1}{\omega+\omega'-\epsilon-\epsilon_p - i\eta}\right)\left(\frac{1}{\omega-\epsilon_q - i\eta}\right) \\ &\propto \int d\epsilon_p \int d\epsilon_q \left(\frac{1}{\omega-\epsilon_p - 3i\eta}\right)\left(\frac{1}{\omega-\epsilon_q - i\eta}\right), \end{aligned} \tag{4.11}$$

and if we assume $\Lambda \gg \omega$, we get

$$\int_{-\Lambda}^{\Lambda} d\epsilon_p \int_{-\Lambda}^{\Lambda} d\epsilon_q \left(\frac{1}{\omega-\epsilon_p - 3i\eta}\right)\left(\frac{1}{\omega-\epsilon_q - i\eta}\right) = (i\pi)(i\pi). \tag{4.12}$$

The precise value is not so important, although it is very easy to get from the above. The important thing to note is that the contribution is non-logarithmic, but also non-zero. This shows the difference between Larsen's and Abrikosov's representations. Here we have to keep diagrams with pf-loops, however, they are not important to this order, if we only look at log-contributions.

To be sure that this is indeed the case for all 3.order diagrams, let us look at the last two, non-parquet-type, diagrams. It is easy to see, by following exactly the same line of reasoning,

[16] See footnote after eq. 3.14.

that

$$g^{(3D)}{}^{21}_{11}(\omega) \propto \iiint \Big[\Big(\tilde{G}^R(\epsilon)\tilde{G}^R(\omega') + \tilde{G}^A(\epsilon)\tilde{G}^A(\omega') \Big) \Big(G^K(\omega+\omega'-\epsilon,\epsilon_p)G^K(\omega+\omega'-\epsilon,\epsilon_q) + G^R(\omega+\omega'-\epsilon,\epsilon_p)G^A(\omega+\omega'-\epsilon,\epsilon_q) \Big) + \Big(\tilde{G}^R(\epsilon)\tilde{G}^A(\omega') + \tilde{G}^A(\epsilon)\tilde{G}^R(\omega') \Big) G^A(\omega+\omega'-\epsilon,\epsilon_p)G^R(\omega+\omega'-\epsilon,\epsilon_q) \Big] . \tag{4.13}$$

The part which we should expect to yield a log-contribution, is the term containing the Keldysh-component of the ce-propagator

$$\begin{aligned} &\int d\epsilon_p \int d\epsilon_q \int \frac{d\epsilon}{2\pi} \int \frac{d\omega'}{2\pi} \Big(\tilde{G}^R(\epsilon)\tilde{G}^R(\omega') + \tilde{G}^A(\epsilon)\tilde{G}^A(\omega') \Big) \\ &\quad \Big(G^K(\omega+\omega'-\epsilon,\epsilon_p)G^K(\omega+\omega'-\epsilon,\epsilon_q) \Big) \\ &= \int d\epsilon_p \int d\epsilon_q \int \frac{d\epsilon}{2\pi} \int \frac{d\omega'}{2\pi} \Big(\tilde{G}^R(\epsilon)\tilde{G}^R(\omega') + \tilde{G}^A(\epsilon)\tilde{G}^A(\omega') \Big) \\ &\quad \big((-2\pi i)\mathrm{sgn}(\epsilon_p)\delta(\omega+\omega'-\epsilon-\epsilon_p)(-2\pi i)\mathrm{sgn}(\epsilon_q)\delta(\omega+\omega'-\epsilon-\epsilon_q) \big) \\ &= \int d\epsilon_p \int d\epsilon_q \int \frac{d\omega'}{(2\pi)^2} \Big(\tilde{G}^R(\omega+\omega'-\epsilon_p)\tilde{G}^R(\omega') + \tilde{G}^A(\omega+\omega'-\epsilon_p)\tilde{G}^A(\omega') \Big) \\ &\quad \Big((-2\pi i)^2 \mathrm{sgn}(\epsilon_p)\mathrm{sgn}(\epsilon_q)\delta(\epsilon_p-\epsilon_q) \Big) \\ &= 0, \end{aligned} \tag{4.14}$$

which is zero since we can close the contour so that there are no poles in the given half-plane when performing the integral over ω'.

The last diagram (3E) from fig 5 is zero due to the fact that we have two traces, and therefore end up with a term like $\tilde{G}^R(\omega')\tilde{G}^R(\omega')$ or $G^R(\omega')G^R(\omega')$, which has poles in only one of the half-planes.

We can see that $\underline{\tilde{G}}$ being diagonal restricts the non-zero terms that we can generate from the Keldysh contraction, and to 3. order they do not contribute with any logarithms. However, they are non-zero in general, and should therefore be considered carefully.

4.3.3 Diagram P_1, P_2, P_3 and P_4

As seen from fig. 5 these diagrams are made by combining parquet-diagrams. We will include the contribution from these by summing up all parquet-type diagrams to infinite order. This is done by requiring our vertex to be independent of the cutoff Λ as we will see now.

4.4 Poor man's scaling - one loop RG

By examining higher order corrections to the vertex, Abrikosov showed that it was only parquet-diagrams, which gave contributions to leading order in log. [5] Abrikosov summed up all of these diagrams using a Dyson-like equation. Here, however, we will use the ideas from RG. It is much

simpler, but it yields the same result.

We want to ensure that the invariant vertex $\tilde{g}$ is independent of the cut-off Λ. This makes sense physically, since we assume $\Lambda \gg T_k, \omega$. If we only include parquet diagrams, i.e. only take second order contributions into account, eq. 4.5 yields

$$\tilde{g} = g\left(1 + 2g\ln\left|\frac{\Lambda}{\omega}\right|\right), \tag{4.15}$$

from which we get

$$\frac{d\tilde{g}}{d\ln(\Lambda)} = \frac{dg}{d\ln(\Lambda)} + 2g^2 + \mathcal{O}(g^3) = 0. \tag{4.16}$$

Now, choosing two limits D_0 and D to evaluate g at, it is readily seen that[17]

$$\left(\frac{1}{2g(D)} - \frac{1}{2g(D_0)}\right) = \ln(D) - \ln(D_0). \tag{4.17}$$

Setting D equal to the temperature T, and defining the Kondo temperature as $T_K = D_0 e^{-\frac{1}{2g(D_0)}}$, we get

$$g(T) = \frac{g(D_0)}{1 - 2\ln\left(\frac{D_0}{T}\right)g(D_0)} = \frac{1}{2\ln\left(\frac{T}{T_k}\right)}. \tag{4.18}$$

We see that for $g > 0$, ie. an antiferromagnetic coupling, the vertex diverges as $T \to T_K$. This result agrees with the one found by Abrikosov [5].

By solving this simple differential equation, we have effectively summed up an infinite series of diagrams. Namely, all the parquet diagrams. This shows why RG is such a powerful method. Instead of solving a Dyson-like equation, we have to solve a differential equation. Now by expanding the denominator as a geometric series, one can see that we indeed generate all parquet-diagrams. The divergence at T_K does not seem to have any physical meaning, so we will now try to get rid of it by including 3. order corrections. This means we go from one-loop RG, or Poor man's scaling, to two loop RG.

4.5 Going beyond Poor man's scaling - two loop RG

Including 3. order corrections from eq. 4.9, the equation for the invariant coupling now becomes

$$\tilde{g} = g\left(1 + 2g\ln\left|\frac{\Lambda}{\omega}\right| - 2g^2\ln\left|\frac{\Lambda}{\omega}\right|\right). \tag{4.19}$$

With two-loop RG we take both leading and subleading diagrams in log into account. Again, since $\tilde{g}$ is independent of the cutoff we get[18]

$$\frac{dg}{d\ln(\Lambda)} = -2g^2 + 2g^3 = 0, \tag{4.20}$$

[17] Here the limits enter the integral $\int_{D_0}^{D}$ as shown explecitly in eq. 4.21.

[18] This result agrees with the one derived by Fowler [8].

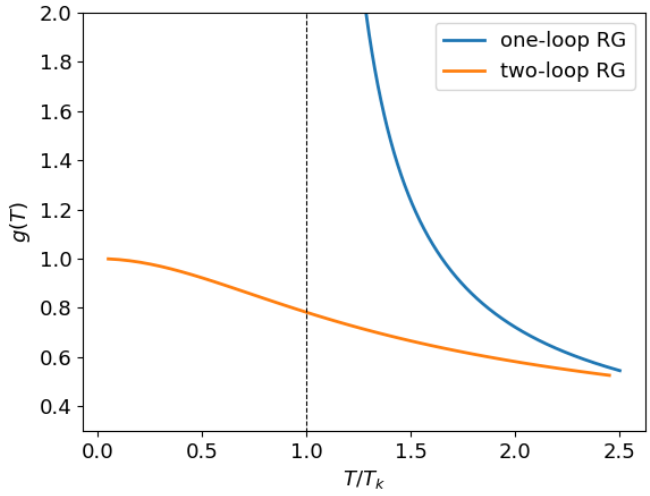

Figure 7: The effective coupling $g(T)$. The dashed line shows $T = T_K$. It is seen that the divergence at T_K in one-loop RG gets eliminated when going to two-loop RG. The two-loop result is found by solving eq. 4.23 numerically in Python.

and taking the integral on both sides, like we did in one-loop RG, we get

$$\ln\left(\frac{T}{D_0}\right) = \int_{g(D_0)}^{g(T)} dg \frac{1}{2g^2(g-1)} = \frac{1}{2}\int_{g(D_0)}^{g(T)} dg \left(\frac{1}{(g-1)} - \frac{1}{g} - \frac{1}{g^2}\right). \tag{4.21}$$

Performing the integral yields

$$\ln\left|1 - \frac{1}{g(T)}\right| + \frac{1}{g(T)} = \ln\left|1 - \frac{1}{g(D_0)}\right| + \frac{1}{g(D_0)} - 2\ln\left(\frac{D_0}{T}\right), \tag{4.22}$$

which we can write as

$$\left(\frac{1}{g(T)} - 1\right)\exp\left(\frac{1}{g(T)}\right) = \left(\frac{1}{g(D_0)} - 1\right)\exp\left(\frac{1}{g(D_0)}\right)\left(\frac{T}{D_0}\right)^2. \tag{4.23}$$

We can see that the divergence at $T = T_K$ is gone, and $g \to 1$ as $T \to 0$. This equation can be solved numerically, and the result can be seen in fig. 7.

5 Perspective and the strong coupling regime

Now that we have seen how Keldysh formalism and Larsen's pseudo-fermions enable us to calculate the vertex in weak coupling, several questions arise. We will treat some of them here.

5.1 Where did the divergence go?

In the 1970's Wilson developed Numerical Renormalization Group (NRG) to treat the Kondo problem. [9] This is a numerical iterative method, where one effectively lowers the temperature at each iteration. Using NRG Wilson showed that if we start out with a small $g > 0$, the coupling will flow from a weak coupling regime at high temperature to a strong coupling regime at

$T \ll T_K$. Since the results of NRG describes experimental data very well, we would like to see the same RG-flow in our model. However, we just found that the divergence did not move from T_K to $T = 0$, but got eliminated completely. This suggests that our perturbation theory breaks down for $T \ll T_K$.

In retrospect this makes sense. Throughout we assumed that $g \ll 1$, so that the perturbative expansion in $g \ln(\Lambda)$ makes sense. But for low T we saw $g \to 1$, and therefore we would expect our perturbation series to break down at this point. We therefore need another way to treat the problem in this strong coupling regime.

The way Wilson did this, with NRG, was to go from ce-states that were localized around the impurity to states that were localized around the Fermi surface, since it is these states that are dominating for $T \ll T_K$. In appendix 8.2 results are shown from an NRG-program that I wrote in Python. This program was made by following Wilson's original article [9], but due to limited space, we will not go into more detail on how the program was made here. However, analytically we are working with an UV-cutoff, which we assume to be very large. So we need another way to deal with this regime.

5.2 Going to strong coupling

We see some new physics when going to the strong coupling regime. The coupling diverges as $T \to 0$, but the ce-states that can be excited, and interact with the impurity spin, are confined close to the Fermi surface. In fact, we would expect the number of these states to be $\propto T^1$.

When the coupling increases in strength, we would expect the conduction electrons to accumulate around the impurity atoms, and as a result the resistance of the metal should increase. This is exactly the effect Kondo tried to explain, so all is good. However, if the coupling diverges, one could argue that the resistance should diverge as well, since all the conduction electrons would be bound to the impurity atoms. But this is not what we find experimentally.

We can explain this by looking at our pf-propagator. When the electrons accumulate around the impurity spin, they will screen the magnetic moment of the impurity spin, and in this way we would expect the impurity to have a finite life-time. We can take this into account by defining the pf-propagator as

$$\underline{\tilde{G}}(\omega) = \begin{bmatrix} \frac{1}{\omega + i\Gamma} & -\frac{2i\Gamma}{\omega^2+\Gamma^2}\mathrm{sgn}(\omega) \\ 0 & \frac{1}{\omega - i\Gamma} \end{bmatrix}, \tag{5.1}$$

and in this way introduce a finite lifetime to the impurity spin. Depending on how g diverges, this Γ could be finite or infinite. In practice, a self-consistent solution for the vertex and the pf-propagator would be needed.[19] This is however beyond the scope of this project. But in principle it could be done, if only a limited number, or types, of diagrams are important at $T \ll T_K$. In that case the Keldysh formalism gives a very nice framework in which we can calculate the value of these diagrams, since, as mentioned before, it comes down to doing tensor contractions and integrals. In this way one could, in theory, write a program that would solve these diagrams self-consistently, and we could likely use this in nonequilibrium problems as well.

[19] If we only go to 2. order we can calculate Γ analytically without doing too much work. This can be seen in appendix 8.3.

5.3 Calculating physical quantities

In the end we do not want to look at the effective coupling, or the lifetime of the impurity spin. We want to calculate physical quantities, such as the resistance of the alloy or the magnetic susceptibility of the spin. If we know the coupling, and the dressed pf-propagator, this would seem quite straightforward. But we have to remember that we are working with Larsen's pseudo-fermions. This means we have a factor $\mathscr{L}$ and $\mathscr{A}$ to worry about as we saw in eq. 3.14. It is not clear how we can calculate these factors exact. Using the definition in 3.4 we get

$$\begin{aligned}\mathscr{L} &= \frac{\mathrm{Tr}^e\left(e^{-\beta H}\right)}{\mathrm{Tr}^s\left(e^{-\beta H}\right)} \\ &= \frac{\frac{1}{2}\,\mathrm{Tr}^e\left(e^{-\beta H(J=0)}\right)}{\mathrm{Tr}^s\left(e^{-\beta H}\right)} + 1 \\ &= \frac{\mathrm{Tr}^s\left(e^{-\beta H(J=0)}\right)}{\mathrm{Tr}^s\left(e^{-\beta H(J)}\right)} + 1, \end{aligned} \tag{5.2}$$

where we have used that spurious states have $S \cdot S = 0$ as noted earlier. From this it is easily seen that $\mathscr{L} = 2$ for $T \gg T_K$. And since the first term is zero for $J \to \infty$, we get $\mathscr{L} = 1$ for $T \ll T_K$. In order to get the value for $\mathscr{L}$ in between these two limits, one would have to look at the partition function in greater detail, or get $\mathscr{L}$ in some other way. Here, however, it is just important to note that this is a complication we have to deal with when using Larsen's pf's.

6 Conclusion

We have seen how Keldysh formalism gives an effective and intuitive framework for working with Feynman diagrams and the Kondo model. We also showed how Larsen's pseudo fermions allow us to represent the impurity spin in terms of fermionic operators, and therefore enable us to use the methods known from QFT such as Wick's theorem. Larsen's pseudo fermions have the great advantage that the chemical potential is zero. This makes the calculations simpler, and we do not have to take the limit where the chemical potential goes to infinity, as Abrikosov had to. However, there are other factors we have to calculate in order to map results from extended to physical Hilbert space.

Using these formalisms, we were able to calculate the vertex to leading and subleading order in log, and to reproduce the results of both Poor man's scaling derived by Abrikosov [5], and the results of two-loop RG [8]. These results gave us an insight into the diagrammatic structure, where diagrams with multiple pf-loops are non-zero in general. However, to 3. order in g, they did not contribute with any logarithms, due to restrictions when contracting the Keldysh-indicies.

Finally, we developed some intuition for the strong coupling regime, and saw how this coupled to the results Wilson got using NRG. This suggests that the coupling should indeed diverge for $T \to 0$, and a lifetime of the impurity spin should be taken into account. However, with a good understanding of the formalism in weak coupling, it seems very likely that the same methods can be used to describe the Kondo model in strong coupling as well.

7 Acknowledgement

I want to give a special thanks to Jens Paaske. This thesis would not have been possible without the discussions and the time that Jens has dedicated to me throughout my studies at NBI.

References

[1] J. Kondo, "Resistance minimum in dilute magnetic alloys," *Progress of theoretical physics*, vol. 32, no. 1, pp. 37–49, 1964.

[2] J. Nygård, D. H. Cobden, and P. E. Lindelof, "Kondo physics in carbon nanotubes," *Nature*, vol. 408, no. 6810, pp. 342–346, 2000.

[3] J. Rammer and H. Smith, "Quantum field-theoretical methods in transport theory of metals," *Reviews of modern physics*, vol. 58, no. 2, pp. 323–359, 1986.

[4] U. Larsen, "A note on the pseudo-fermion representation of a spin 1/2 or 1," *Zeitschrift für Physik A Hadrons and nuclei*, vol. 256, no. 1, pp. 65–72, 1972.

[5] A. Abrikosov, "Electron scattering on magnetic impurities in metals and anomalous resistivity effects," *Physics Physique Fizika*, vol. 2, no. 1, pp. 5–20, 1965.

[6] W. Götze and P. Wölfle, "Dynamical impurity spin susceptibility in metals," *Journal of Low Temperature Physics*, vol. 5, no. 5, pp. 575–589, 1971.

[7] A. Jauho, "Introduction to the keldysh nonequilibrium green function technique," *Lect. notes*, vol. 17, 2006.

[8] M. Fowler and A. Zawadowski, "Scaling and the renormalization group in the kondo effect," *Solid State Communications*, vol. 9, no. 8, pp. 471–476, 1971.

[9] K. G. Wilson, "The renormalization group: Critical phenomena and the kondo problem," *Reviews of modern physics*, vol. 47, no. 4, pp. 773–840, 1975.

8 Appendices

8.1 Calculating the vertex contribution from diagram 3A

Here we give the derivation of $g^{(3A)}$. From eq. 4.6 we have

$$
\begin{aligned}
&g^{(3A)}{}^{21}_{11}(\omega)\frac{i}{4}\sum_k \tau^k_{\sigma'\sigma}\tau^k_{\gamma'\gamma} \\
&\quad= \left(\frac{i}{4}\right)^3(-1)\sum_{i_1,i_2,i_3}\left[\tau^{i_1}\tau^{i_2}\tau^{i_3}\right]_{\gamma'\gamma}\mathrm{Tr}\left[\tau^{i_1}\tau^{i_3}\right]\tau^{i_2}_{\sigma'\sigma}\int d\epsilon_p\int d\epsilon_q\int\frac{d\epsilon}{2\pi}\int\frac{d\omega'}{2\pi}g^3 \\
&\quad\Big[\left(\tilde{G}^R(\omega+\omega'-\epsilon)\tilde{G}^R(\omega+\omega'-\epsilon)\right)\Big(G^R(\omega',\epsilon_p)G^A(\epsilon,\epsilon_q) \\
&\qquad+G^A(\omega',\epsilon_p)G^R(\epsilon,\epsilon_q)+G^K(\omega',\epsilon_p)G^K(\epsilon,\epsilon_q)\Big) \\
&\quad+\left(\tilde{G}^A(\omega+\omega'-\epsilon)\tilde{G}^A(\omega+\omega'-\epsilon)\right)\Big(G^R(\omega',\epsilon_p)G^R(\epsilon,\epsilon_q)+G^A(\omega',\epsilon_p)G^A(\epsilon,\epsilon_q)\Big)\Big].
\end{aligned}
\tag{8.1}
$$

The last term yields zero, since it only contains poles in upper or lower half-plane, so when closing the contour we can make this zero. The same goes for the first part of the first term. So, upon performing the sum over the Pauli matrices, we get

$$
\begin{aligned}
&= \left(\frac{i}{4}\right)^3(-1)\sum_k\left((-2)\tau^k_{\sigma'\sigma}\tau^k_{\gamma'\gamma}\right)\int d\epsilon_p\int d\epsilon_q\int\frac{d\epsilon}{2\pi}\int\frac{d\omega'}{2\pi}g^3 \\
&\left(\tilde{G}^R(\omega+\omega'-\epsilon)\tilde{G}^R(\omega+\omega'-\epsilon)\right)\Big(G^A(\omega',\epsilon_p)G^R(\epsilon,\epsilon_q)+G^K(\omega',\epsilon_p)G^K(\epsilon,\epsilon_q)\Big) \\
&= \left(\frac{i}{4}\right)^3\sum_k\left(2\tau^k_{\sigma'\sigma}\tau^k_{\gamma'\gamma}\right)\int d\epsilon_p\int d\epsilon_q\int\frac{d\epsilon}{2\pi}\int\frac{d\omega'}{2\pi}g^3 \\
&\left(\tilde{G}^R(\omega+\omega'-\epsilon)\tilde{G}^R(\omega+\omega'-\epsilon)\right)\Big(G^K(\omega',\epsilon_p)G^K(\epsilon,\epsilon_q)\Big)\left(1-\mathrm{sgn}(\epsilon_p)\mathrm{sgn}(\epsilon_q)\right) \\
&= \left(\frac{i}{4}\right)^3\sum_k\left(2\tau^k_{\sigma'\sigma}\tau^k_{\gamma'\gamma}\right)\int_{-\Lambda}^{\Lambda}d\epsilon_p\int_{-\Lambda}^{\Lambda}d\epsilon_q\int\frac{d\epsilon}{2\pi}\int\frac{d\omega'}{2\pi}g^3 \\
&\left(\frac{1}{(\omega+\omega'-\epsilon+i\eta)^2}\right)\Big((-2i\pi)^2\delta(\omega'-\epsilon_p)\delta(\epsilon-\epsilon_q)\Big)\left(\mathrm{sgn}(\epsilon_p)\mathrm{sgn}(\epsilon_q)-1\right) \\
&= \left(\frac{i}{4}\right)^3\sum_k\left(2\tau^k_{\sigma'\sigma}\tau^k_{\gamma'\gamma}\right)\int_{-\Lambda}^{\Lambda}d\epsilon_p\int_{-\Lambda}^{\Lambda}d\epsilon_q g^3\left(\frac{(-1)}{(\omega+\epsilon_p-\epsilon_q+i\eta)^2}\right)\left(\mathrm{sgn}(\epsilon_p)\mathrm{sgn}(\epsilon_q)-1\right)
\end{aligned}
$$

$$
\begin{aligned}
&= \left(\frac{i}{4}\right)^3\sum_k\left(2\tau^k_{\sigma'\sigma}\tau^k_{\gamma'\gamma}\right)\int_0^{\Lambda}d\epsilon_p\int_0^{\Lambda}d\epsilon_q g^3\left(\frac{2}{(\omega+\epsilon_p+\epsilon_q+i\eta)^2}+\frac{2}{(\omega-\epsilon_p-\epsilon_q+i\eta)^2}\right) \\
&= \left(\frac{i}{4}\right)^3\sum_k\left(2\tau^k_{\sigma'\sigma}\tau^k_{\gamma'\gamma}\right)g^3\left(2\ln\left|\frac{\Lambda^2-\omega^2}{\omega^2}\right|-2\ln\left|\frac{4\Lambda^2-\omega^2}{\Lambda^2-\omega^2}\right|\right),
\end{aligned}
\tag{8.2}
$$

which gives us the final result

$$g^{(3A)}{}^{21}_{11}(\omega)\frac{i}{4}\sum_k \tau^k_{\sigma'\sigma}\tau^k_{\gamma'\gamma} = \left(\frac{i}{4}\right)^3 \sum_k \left(2\tau^k_{\sigma'\sigma}\tau^k_{\gamma'\gamma}\right) g^3 \left(2\ln\left|\frac{\Lambda^2-\omega^2}{\omega^2}\right| - 2\ln\left|\frac{4\Lambda^2-\omega^2}{\Lambda^2-\omega^2}\right|\right). \quad (8.3)$$

8.2 Numerical renormalization group code and results

Following Wilsons article on the Numerical Renormalization Group [9] a program was made that runs NRG for the Kondo model. I wrote the program in Python and used Wilson's results as a benchmark. We will not go into detail on how NRG works, but the main idea is to look at the Kondo model perturbatively. We start by looking at high energy scales. Here the ce-states in the metal located close to the impurity atom are important. We then diagonalize the Hamiltonian, and use the resulting states as our new basis. At each iteration we go to lower energy scales. This is done by including states that are closer to the Fermi surface. It is these states that dominate the low energy physics of the system. In essence the method is very similar to how one would calculate the fine structure of the Hydrogen atom.

There are a lot of technical details on how this is done, but one starts by writing the Kondo model in terms of a hopping Hamiltonian, and in this way maps the Kondo model to a semi-infinite chain. At each iteration we add an extra site to this chain, corresponding to going to lower energies.

The first few energy states generated by the code are shown in fig. 8. After around 25 iterations the energies of the excited states have converged. Actually the energies at even and odd iterations converge towards different values. The code yielded [20]

$$\begin{aligned} \text{Even iterations: } & 0.6555117 \pm 2\times10^{-7}, \quad 1.3110240 \pm 3\times10^{-7}, \quad 1.9760011 \pm 3\times10^{-7}, \quad ... \\ \text{Odd itertaions: } & 1.2963851 \pm 2\times10^{-7}, \quad 2.5927712 \pm 3\times10^{-7}, \quad 2.8259709 \pm 7\times10^{-7}, \quad ... \end{aligned}$$

Wilson showed that for $J \to \infty$, the energies of the states are given by

$$\begin{aligned} \text{Even iterations: } & 0.6555, \quad 1.3110, \quad 1.976, \quad ... \\ \text{Odd itertaions: } & 1.297, \quad 2.594, \quad 2.827, \quad ... \end{aligned}$$

agreeing well with the results obtained from the NRG-program. Note that the uncertainties are simply the standard deviation of the mean. But this is clearly not "independent measurements", since we only look at a single run, with the same parameters for J etc. so we should not be worried about the results for the odd iterations lying many std's away from the theoretical prediction made by Wilson. The important thing to note is that, even if we start out with a small positive value J, when we go to the low energy limit, we indeed end up in the strong coupling regime where J diverges.[21]

[20] As seen from fig. 8 there is a degeneracy at each energy level. I used this degeneracy to calculate the mean of each energy level, and in this way got an uncertainty as well. However, a more thorough analysis of uncertainties is needed.

[21] We do not give the parameters used for this specific run of the NRG-code. This is because many parameters are given beyond the coupling, such as the number of states kept after each iteration, the fraction with which we decrease the energy scale after each iteration etc. See Wilson's article for more on this. [9]

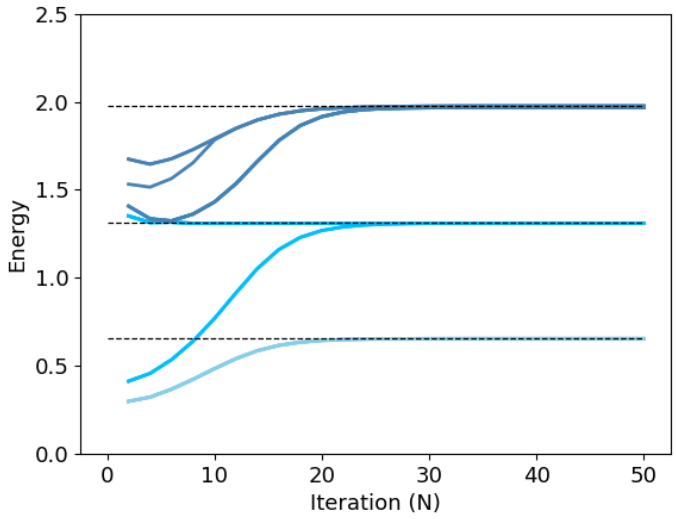

Figure 8: The RG-flow of the lowest energy levels at even iterations N. The results are from a NRG-code which was made by following Wilson's article on NRG [9]. The dashed lines are the theoretical prediction for the energies at $J = \infty$ made by Wilson. We see that the energies converge towards the results expected when $J = \infty$, indicating that the effective coupling g indeed does diverge as $T \to 0$. Note that the lowest energy levels are rescaled after each iteration, otherwise they would just decrease, and converge to zero as $N \to \infty$.

8.3 Calculating the pseudo-fermion relaxation rate to 2. order in g

To 2. order in g, the relaxation rate Γ is given by two ce-propagators forming a loop together with a pf-propagator. Writing Γ in terms of the pf self-energy, Σ, and representing the loop consisting of one pf- and one ce-propagator by $\mathcal{I}$,[22] we get

$$
\begin{aligned}
\Gamma &= \frac{i}{2}\left(\Sigma^R - \Sigma^A\right) = \frac{i}{2}\left(\Sigma^> - \Sigma^<\right) \\
&= \left[\frac{i}{2}\right]\left[g^2(-1)\left(\frac{i}{2^2}\right)^2\right]\left[6\delta_{\gamma\gamma'}\right]\int d\epsilon_p \int d\epsilon_q \int \frac{d\omega'}{2\pi}\left(I^<(\omega',\epsilon_p)G^>(\omega',\epsilon_q) - I^>(\omega',\epsilon_p)G^<(\omega',\epsilon_q)\right) \\
&= \left[\frac{i}{2}\right]\left[g^2(-1)\left(\frac{i}{2^2}\right)^2\right]\left[6\delta_{\gamma\gamma'}\right]\int d\epsilon_p \int d\epsilon_q \int \frac{d\omega'}{2\pi}\left[\pi n_f(\epsilon_p)\delta(\omega'-\epsilon_p)(-2\pi i)n_f(-\epsilon_q)\delta(\omega'-\epsilon_q)\right. \\
&\qquad\qquad \left. -\pi n_f(-\epsilon_p)\delta(\omega'-\epsilon_p)(2\pi i)n_f(\epsilon_q)\delta(\omega'-\epsilon_q)\right] \\
&= \left(\frac{i}{2}\right) g^2 \frac{\pi}{16}\left(6\delta_{\gamma\gamma'}\right)\int d\epsilon_p(-i)\left[n_f(\epsilon_p)n_f(-\epsilon_p) + n_f(-\epsilon_p)n_f(\epsilon_p)\right] \\
&= \frac{3\pi}{8} g^2 \delta_{\gamma\gamma'} \int_{-\infty}^{\infty} \frac{1}{e^{\beta\epsilon_p}+1}\frac{1}{e^{-\beta\epsilon_p}+1} \\
&= \frac{3\pi}{8}\delta_{\gamma\gamma'} g^2 k_b T. \qquad (8.4)
\end{aligned}
$$

We see that due to the Kondo-interaction we get a non-zero Γ. Note that g diverges at $T \to 0$, so it is possible to get a nonzero Γ at $T = 0$.

[22] The loop, $\mathcal{I}$, is just like the one seen in diagram 2P in fig. 6.